JASA ARTICLE

# The physics of knocking over LEGO minifigures with time reversal focused vibrations for use in a museum exhibit[a)]

Lucas A. Barnes,[1] Brian E. Anderson,[1,b)] Pierre-Yves Le Bas,[2] Adam D. Kingsley,[1] Aaron C. Brown,[1] and Henrik R. Thomsen[3]

[1]*Acoustics Research Group, Department of Physics and Astronomy, Brigham Young University, N283 Eyring Science Center, Provo, Utah 84602, USA*

[2]*Detonator Science and Technology (Q-6), Los Alamos National Laboratory, MS D446, Los Alamos, New Mexico 87545, USA*

[3]*Department of Earth Sciences, Eidgenössische Technische Hochschule Zürich, Zürich 8092, Switzerland*

**ABSTRACT:**

Time reversal (TR) is a method of focusing wave energy at a point in space. The optimization of a TR demonstration is described, which knocks over one selected LEGO minifigure among other minifigures by focusing the vibrations within an aluminum plate at the target minifigure. The aim is to achieve a high repeatability of the demonstration along with reduced costs to create a museum exhibit. By comparing the minifigure's motion to the plate's motion directly beneath its feet, it is determined that a major factor inhibiting the repeatability is that the smaller vibrations before the focal event cause the minifigure to bounce repeatedly and it ends up being in the air during the main vibrational focal event, which was intended to launch the minifigure. The deconvolution TR technique is determined to be optimal in providing the demonstration repeatability. The amplitude, frequency, and plate thickness are optimized in a laboratory setting. An eddy current sensor is then used to reduce the costs, and the impact on the repeatability is determined. A description is given of the implementation of the demonstration for a museum exhibit. This demonstration illustrates the power of the focusing acoustic waves, and the principles learned by optimizing this demonstration can be applied to other real-world applications. © *2022 Acoustical Society of America*.

https://doi.org/10.1121/10.0009364

(Received 22 September 2021; revised 5 January 2022; accepted 7 January 2022; published online 3 February 2022)

[Editor: James F. Lynch] Pages: 738–751

## I. INTRODUCTION

Time reversal (TR) is a wave focusing method, which can be used to achieve spatial focusing.[1–3] The process involves reversing an impulse response obtained between two points in space and emitting it from one of these locations such that the waves constructively interfere at the other location. In fact, the time reversed impulse response (TRIR) may be emitted from either location, and the same focusing signal will result at the other location because of the acoustic reciprocity in a linear, time-invariant environment.

TR was originally called matched signal processing and developed for underwater acoustic applications.[4,5] During the traditional TR process, waves sent through the system are affected by the transfer function of the system during the forward step (when the impulse response is obtained) and again during the backward step (the broadcast of the TRIR). This double filtering of the system (the matched signal process) decreases the spatial resolution of the TR focusing and introduces relatively high temporal sidelobes compared to the focus peak, which reduce the quality of focus. One solution to this issue is a TR method termed inverse filtering or deconvolution TR,[6–9] which compensates for the forward step transfer function prior to the backward step. This provides improved spatial and temporal confinement when the TR focusing is impulsive in nature but at the cost of a reduced TR focusing amplitude. Other uses include energy focusing, secure communications, and source imaging. As an example of energy focusing, TR has been used to focus ultrasonic waves to the location of kidney stones to break them into smaller pieces non-intrusively.[10,11] TR is used to generate high-amplitude energy focusing of loud audible sound in a room,[12] ultrasound to generate a difference frequency,[13] and to excite structures with focused sound.[14,15] In communications applications, TR is used to send a private message that would only be discernable at the target location, whereas elsewhere it would just sound like noise.[4,16–19] TR can also be used to image earthquakes[20–23] and aero-acoustic sources[24–26] by modeling the propagation of time reversed recordings. TR has been used in nondestructive evaluation applications to focus energy to various points of interest to locally quantify the nonlinear response of those points, which allows cracks and defects to be imaged because they are the sources of that nonlinear response.[3,27–29]

One demonstration of TR acoustics was presented by Fink[30] in 1999. In the demonstration, an array of loudspeakers and microphones were used, which is called a TR mirror, to record sounds, reverse them, and then focus the reversed sounds back to their source. If a person stood in front of the array and said "hello," the TR mirror would focus the sound as "olleh" back to the person's mouth,

[a)]This paper is part of a special issue on Education in Acoustics.

[b)]Electronic mail: bea@byu.edu, ORCID: 0000-0003-0089-1715.

 

https://doi.org/10.1121/10.0009364

where the sound originated. It is stressed in the paper that the sound is not just being retransmitted to spread out into the room like normal sound, and instead it converges only at the person's mouth via the constructive interference of waves generated by the loudspeaker array and the virtual array made up of the appropriately timed reflections from the room boundaries.

In another demonstration by de Mello *et al.*,[31] TR was used to focus the surface water waves in a tank. The border of the tank was lined with 148 transducers, which could record the incoming waves and then emit the reversed recordings of them. For their TR experiments, first, an object was dropped into the tank as an impulsive source of the surface waves. The transducers recorded the reflections of the waves off of the sides of the tank and then after the water had settled, the reversed recordings were broadcast, causing the waves to converge at the original source location and create a focused motion of the surface, which was clearly visible to observers.

More recently, Heaton *et al.*[32] developed a visual demonstration of TR focused vibrations in a thin plate. A single vibration speaker or shaker was used to excite the vibrations in the plate after which a scanning laser Doppler vibrometer (SLDV) was used to quantify the reverberation time and vibration coupling efficiency from the shaker to the plates. The various plate materials were tested to explore the possible spatial confinement of the TR focus as well as the highest focal amplitude possible in the different plates. They found that glass, while fragile, provided the highest coupling efficiency and focal amplitude at the lowest cost, whereas aluminum provided results that were nearly as good while being much more durable. To demonstrate the focusing visually, salt was distributed on the plate. Using a slow-motion camera, the observers could then see the salt thrown off the plate at the location and time of the focus, whereas the salt elsewhere on the plate stayed mostly in contact with the plate during the focus. Additionally, some small objects, such as cardboard cylinders, wooden corks, and LEGO minifigures, could be placed at the focal location and knocked over (fall onto ones side) during the focus but not knocked over when placed away from the focal location. However, the ability to knock over the target object was not repeatable enough to use for a consistent demonstration (this is known because B.E.A. was a coauthor on the work of Heaton *et al.*[32]). Their work focused mainly on achieving the highest possible focal amplitude for the purpose of creating a visual demonstration of TR focusing, but they did not optimize the repeatability of knocking over small objects at the focal location. This resulted in a very loud and shrill sounding demonstration, which sometimes launched an object, such as a minifigure, several centimeters into the air before falling over and sometimes only made the object rattle on top of the plate, but it would remain standing.

This paper expands on the results of Heaton *et al.*[32] to create a more repeatable, interactive, user-friendly demonstration of TR focusing for a museum exhibit. Because the demonstration would be in an exhibition hall, reducing the audible noise of the demonstration was also a goal. A 100% reliable means of knocking over a target LEGO minifigure while leaving surrounding minifigures standing is determined in this work by using the TR inverse filter (or deconvolution) method at an optimal excitation level from the multiple shakers. Previously, the repeatability of knocking over a target LEGO minifigure with TR acoustics in a thin aluminum plate was around 30%, which was not previously reported by Heaton *et al.* An explanation is given here for why the target minifigure might not be knocked over despite a sufficiently large TR focal amplitude. The work of Heaton *et al.* focused on obtaining the largest possible peak focal amplitude through the use of the clipping TR (a variant of one-bit TR[33,34]), whereas, here, it is shown that the higher temporal quality of the TR focusing obtained with the deconvolution TR is critical to the successful repeatability of this demonstration. Additionally, a much less expensive noncontact vibration sensor is used to make the demonstration more practical in its implementation.

This paper will first describe the physics behind the main issue with creating a repeatable demonstration. A discussion of the experiments conducted to optimize the demonstration will then be given. The optimal plate thickness, frequency bandwidth, and input voltage to the shakers are explored. Then the use of an eddy current sensor (ECS) instead of a laser Doppler vibrometer is optimized. This paper explores the use of a velocity sensor versus using a displacement sensor to create the TR focusing of the plate's velocity or displacement. Finally, the details are provided about how the demonstration was adapted for an exhibit at a wave propagation museum, which is planned to be hosted at ETH University in Zurich, Switzerland.

## II. UNDERSTANDING THE TR LEGO DEMONSTRATION

The experimental setup used to create the results discussed in this section and Fig. 1 consists of a 1.27 mm thick aluminum plate which is elevated 2 cm above an optical table by four rubber stoppers placed at the corners of the plate. Custom LabVIEW software (Austin, TX) is used to create a logarithmic chirp signal with a bandwidth of 100–2000 Hz, which lasts 0.5 s with 0.3 s of leading zeros and 0.2 s of trailing zeros. A 14-bit 4-channel Spectrum M2i.6022-exp generator card is used to output the chirp signal to one Mighty Dwarf 7W shaker (Milton, ON, Canada). The acquisition is done with a Polytec PSV-400 SLDV (Baden-Württemberg, Germany) and a 16-bit 4-channel Spectrum Instrumentation GmbH M2i.4931-exp digitizer card (Grosshansdorf, Germany) with a sampling frequency of 30 kHz. The SLDV is mounted above the plate and aimed at a patch of retroreflective tape on top of the plate. The impulse response is measured, normalized, and reversed in time and then any additional signal processing techniques, such as the clipping TR or deconvolution TR, are implemented. Finally, the resultant signal is broadcast from the shaker, creating a focus at the location where the SLDV measured the impulse response.

Heaton *et al.*[32] used the clipping TR and deconvolution TR together in an attempt to generate the largest focal amplitude possible, thinking that this was the only important

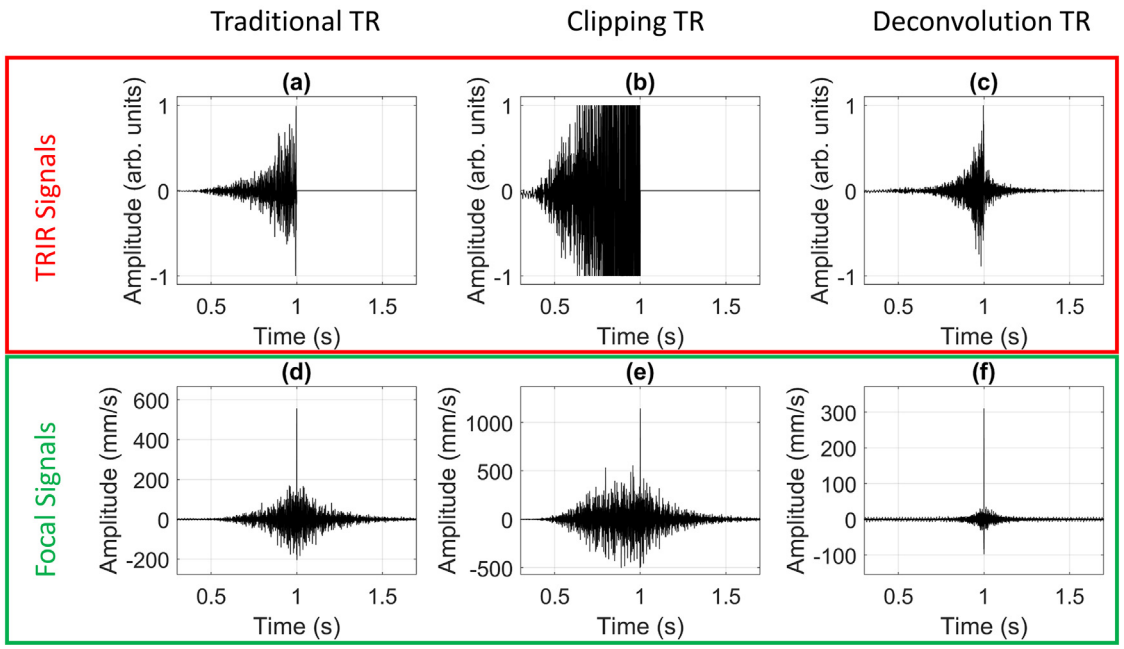


FIG. 1. (Color online) The TRIRs, including the modified ones, are displayed in the (a) traditional TRIR, (b) clipping TRIR, and (c) deconvolution TRIR. The focal signals obtained with these respective TRIR signals are displayed in the (d) traditional TR focus, (e) clipping TR focus, and (f) deconvolution TR focus. Note the differences in the ranges of the ordinate axes of the focal signals in (d)–(f).

goal for a repeatable demonstration of the localized focusing. However, as will be presented in this section, there were problems with the technique they used. To illustrate these issues, we will discuss the basics of the traditional TR, clipping TR, and deconvolution TR and discuss a critical finding that was made, which helped explain why the method used by Heaton *et al.* was not optimal for high repeatability. Their technique launches LEGO minifigures very high into the air but it is not very repeatable. The deconvolution TR technique can be used to obtain high repeatability of launching the LEGO but perhaps not quite with the same altitude. We will repeat the technique used by Heaton *et al.* along with some further measurements to illustrate its flaws along with similar measurements on the optimal deconvolution TR technique.

### A. Traditional TR

In the traditional TR, a signal $s(t)$ is broadcast from a source into a system. A convolution of $s(t)$ with the impulse response of the system, $h(t)$, represents the response signal, $r(t)$, which would be recorded at some receiver location in the system

$$s(t) * h(t) = r(t). \tag{1}$$

If $s(t)$ is an impulsive signal, such as a delta function, $\delta(t)$, then $r(t) = h(t)$, and it can be used with further signal processing to achieve different types of TR focusing. Although this direct measurement of $h(t)$ seems theoretically easy to accomplish, it is difficult for realistic sources to produce a perfect impulse and attempts to do so result in a poor signal-to-noise ratio. Instead, the chirp method is used to indirectly obtain the impulse response.[35,36] In this method, a chirp or sweep through a range of frequencies is broadcast into the system as $s(t)$. The response to the chirp, $r(t)$, can then be –cross correlated with the chirp to produce a band limited impulse response, $h(t)$.

Once $h(t)$ is obtained, reversing it in time and broadcasting $h(-t)$ into the system yields

$$h(-t) * h(t) = y(t), \tag{2}$$

meaning that $y(t)$ is an autocorrelation result—a time-symmetric signal with a peak at the center—which corresponds to the peak focused amplitude that is characteristic of the TR process.[6] The method just described, simply broadcasting an unmodified $h(-t)$ is what we will refer to as the traditional TR. Two variants of TR, which were mentioned in the Introduction, the clipping TR and deconvolution TR, will now be described.

### B. Clipping TR

The aim of the clipping TR method is to maximize the peak amplitude delivered to the focal location. The method is similar to the traditional TR except that before the reversed and normalized impulse response is broadcast into the system, a clipping threshold $C$ is defined between zero and one. Then, every data point in the normalized impulse response that has a value $>C$ is set equal to $C$ and every data point that has a value $< -C$ is set equal to $-C$. The clipped signal is then normalized such that the clipped portions of the signal are at $\pm 1$. The clipping of the signal alters the amplitude of the wave arrivals in the impulse response, but the timing of the waves is still preserved. Thus, the

https://doi.org/10.1121/10.0009364

waves that are emitted in this clipped TRIR have a much larger relative amplitude than when using a traditional TRIR, and the amplitude is increased at the focal location. Figure 1 shows a comparison between a traditional TRIR in Fig. 1(a) and a clipping TRIR in Fig. 1(b) along with their corresponding focal signals, Figs. 1(d) and 1(e), respectively. As seen in a comparison of the signals displayed in Figs. 1(d) and 1(e), the clipping TR method creates a higher peak amplitude focus but at the cost of a lower signal-to-noise ratio (the peak amplitude compared to the amplitudes elsewhere).

### C. Deconvolution TR or inverse filtering

The deconvolution or inverse filtering TR method seeks to maximize the signal-to-noise ratio of the focal signal by compensating for the resonances of the system. When the chirp signal described previously is broadcast into the system, its frequency content is affected by the resonances of the system transfer function, $H(f) = \mathcal{F}\{h(t)\}$, where $\mathcal{F}$ represents a Fourier transform operation. During the traditional TR, with an impulsive signal, the focal signal is equivalent to an autocorrelation of $h(t)$ or an autospectrum of $H(f)$. This means that the system resonances impact the focal signal during the forward and backward steps of the TR, hence, this is why the TR was originally called a matched signal process.[4,5] To compensate for these resonances, the inverse filter (or inverse transfer function) of the system $H^{-1}(f)$ is computed and then transformed into the time domain, normalized, time reversed, and broadcast into the system. When this modified impulse response is sent into the system, the inverse filter mixes with the resonances of the system, resulting in a relatively constant frequency response,

$$H(f)^{-1} * H(f) = 1. \tag{3}$$

The inverse filter or deconvolution TRIR [Fig. 1(c)] results in a focal signal with a lower peak amplitude than the traditional TR but yields a much better signal-to-noise ratio [Fig. 1(f)] than was achieved with the traditional TR or clipping TR.

### D. TR technique optimization for high repeatability

Both the clipping TR and deconvolution TR were combined by Heaton *et al.*[32] by first calculating the deconvolution TRIR and then applying the clipping TR method to that signal before broadcasting it. This was used to achieve a moderately clean focus signal but with a higher peak amplitude focus than in the results with the deconvolution TR by itself. Despite having a high amplitude focus that could easily knock over a LEGO minifigure (an example result is shown in Fig. 2), an attempt to replicate the experiment using this method and a somewhat lower input amplitude and a thinner plate, resulted in a repeatability of 45% in the success rate of knocking over the target LEGO minifigure when performed on an aluminum plate with 2 shakers for a set of 40 trials. The LEGO minifigure might be launched up to 4 cm into the air before falling down 45% of the time. The rest of the time, the target LEGO minifigure would visibly vibrate (rattle on the plate surface) and rotate a bit, but it would not be launched into the air and instead would remain standing. The thickness of the plate used in these experiments, 1.27 mm, was smaller than that of the plates used in Heaton's experiments, which contributed to a slightly higher repeatability than the approximate 30% repeatability that Heaton *et al.* experienced. The optimization of the plate thickness is discussed in Sec. III.

To understand the reason for this low degree of repeatability, a SLDV was aimed at the top of a target LEGO minifigure's feet to measure the velocity over time of the minifigure during a broadcast of the TRIR. Then the experiment was repeated with the SLDV aimed to measure the velocity of the plate below its feet. The plate velocity recorded during the deconvolution plus the clipping TR and during deconvolution TR focusing is shown in Figs. 3(a) and 3(b), respectively. The velocity of the minifigure's feet during each of these focusing events is shown in Figs. 3(c) and 3(d), respectively. In Fig. 3(c), there are several abrupt increases in the velocity with each followed by a consistent downward sloping velocity, whose slope corresponds to the acceleration resulting from the gravity. Thus, it was discovered that the minifigure was repeatedly losing contact with the top of the plate for just a few milliseconds at a time but with enough vertical displacement from the plate to often miss the main focal event entirely. This discovery led to the critical understanding that if the smaller vibrations leading up to the focal event (termed sidelobes in the TR literature) were high enough in amplitude, they would cause the minifigure to lose contact with the plate and, thus, decrease the

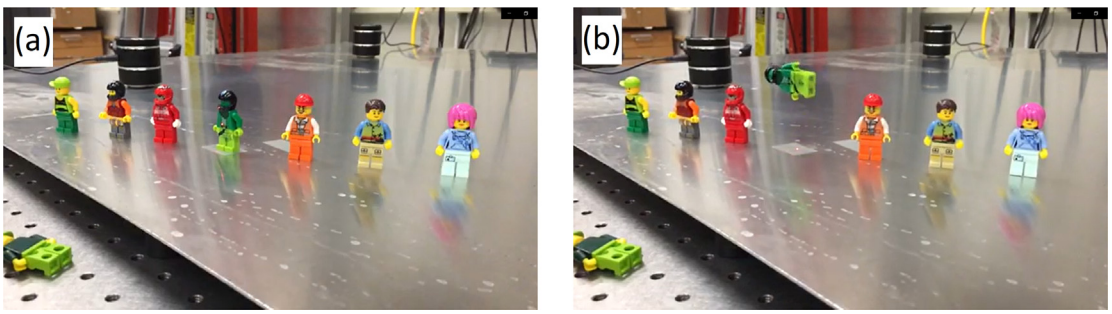


FIG. 2. (Color online) The (a) setup of the LEGO demonstration with two shakers in the background and the SLDV aimed (from above the plate) at the minifigure in the middle and (b) airborne minifigure after the focus are shown.

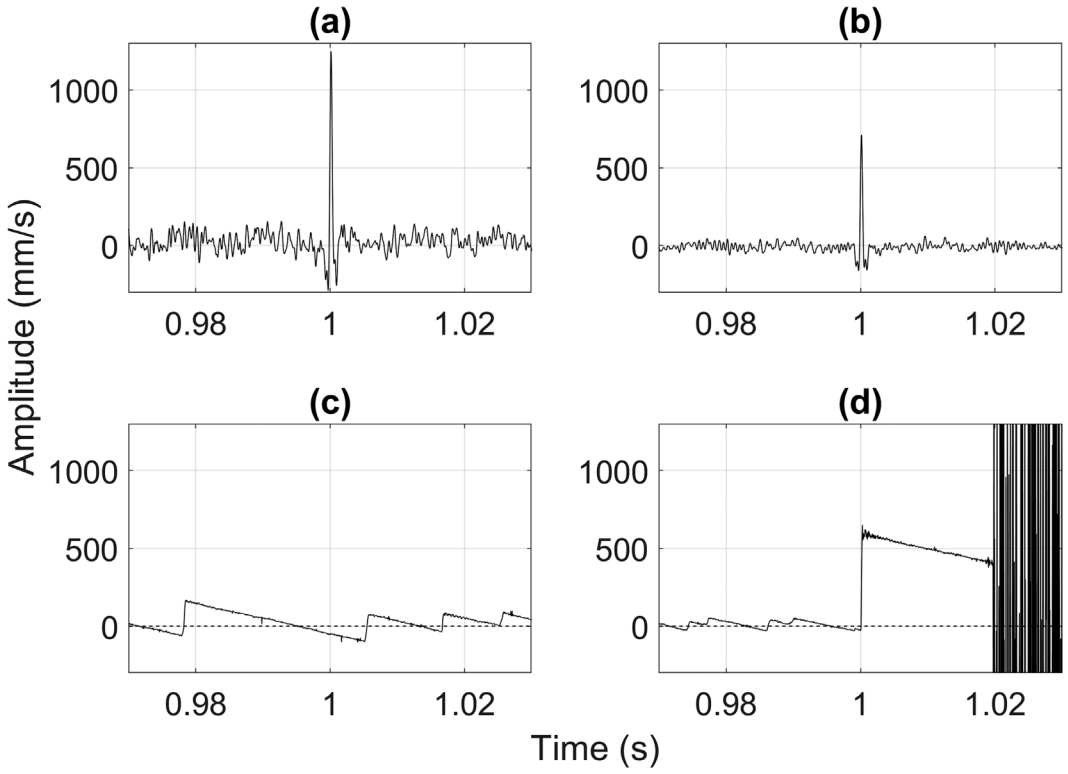


FIG. 3. The (a) plate velocity during the deconvolution plus the clipping TR focusing, (b) plate velocity during the deconvolution TR focusing, (c) LEGO minifigure velocity measured at their feet during the deconvolution plus clipping TR, and (d) LEGO minifigure velocity measured at their feet during the deconvolution TR are shown.

chances of the minifigure being knocked over by the main focal event.

With this understanding in mind, it is clear that a better approach to increasing the repeatability of the demonstration is to use the cleanest TR method possible, such as only deconvolution the TR without any clipping to minimize the amplitude of the sidelobes while maintaining enough amplitude in the focus to launch the minifigure. The repeatability experiment was performed again, this time only using the deconvolution TR, and the resulting repeatability was 75% for a set of 40 trials. Figure 3 shows a comparison between the clipping TR and deconvolution TR focal signals and examples of how the LEGO minifigures react to those signals. All further experiments discussed use the deconvolution TR.

## III. OPTIMIZING THE DEMONSTRATION IN A LABORATORY

A set of experiments were designed and performed to optimize the parameters of the demonstration for increased repeatability. These included the plate thickness, chirp frequency range and bandwidth, and TRIR amplitude.

### A. Plate thickness

While Heaton *et al.*[32] explored the use of different types of plate materials for the demonstration, the thickness of the plate was not previously explored. The TR experiments were performed on three different aluminum plates, whose thicknesses were 6.35 mm, 3.18 mm, and 1.27 mm. The dimensions of the 6.35 mm and 3.18 mm thick plates were 0.91 m × 1.22 m. The 1.27 mm thick plate was initially the same dimensions but was cut and bent into the shape of a bridge, which is the same shape that was used in the museum exhibit. The plate thickness is expected to play a more significant role in the trends observed than the plate's shape or area. Four shakers were used with their amplification settings at maximum on each plate along with a chirp bandwidth of 100–2000 Hz. The shakers were placed near the corners of the plate, but the shaker position was not explored in detail. Two metrics were used to quantify the results: temporal quality and peak amplitude. For these experiments, the temporal quality is defined[32,37] as

$$\xi_T = \frac{[A_P]^2}{\sqrt{\frac{1}{M}\sum_{m=1}^{M}\left[A(x_0, y_0, z_0, m)\right]^2}}, \tag{4}$$

where $A_P$ is the peak amplitude at the focus location, $A(x_0, y_0, z_0, m)$ is an amplitude measurement at the focal location, $(x_0, y_0, z_0)$, at a given time sample $m$, and $M$ is the total number of time samples in the signal. $\xi_T$ provides a relative indication of the focal amplitude as compared to the sidelobe amplitudes. Because high amplitude sidelobes are undesirable, a high $\xi_T$ is desired. As the plate thickness decreased, several trends were noticed. As indicated in Table I, the smaller plate thickness yields both a higher peak

https://doi.org/10.1121/10.0009364

TABLE I. The experimentally obtained results when using TR in the different thickness aluminum plates for the peak amplitude of the TR focusing, $A_P$, and temporal quality, $\xi_T$.

| Thickness (mm) | $A_P$ (mm/s) | $\xi_T$ |
|---|---|---|
| 6.35 | 96 | 60.2 |
| 3.18 | 662 | 69.4 |
| 1.27 | 1490 | 73.9 |

amplitude as well as a higher temporal quality, which are both desirable traits for the TR focusing.

Another noticeable trend was that when the demonstration uses a thicker plate, the sound radiated by the plate is louder and has a shrill sound quality, which is undesirable for the demonstrations. The bending waves (or zeroth-order, antisymmetric Lamb waves) in the plate, which are assumed to dominate in these experiments, are dispersive. The phase speed of these bending waves, $c_b$, is proportional to the square root of the frequency, $f$ (and angular frequency, $\omega = 2\pi f$), and proportional to the square root of the plate thickness, $h$,

$$c_b = \left(\frac{\omega^2 E h^2}{12\rho(1-\nu^2)}\right)^{1/4}, \tag{5}$$

where $E$ is Young's modulus, $\rho$ is the mass density, and $\nu$ is Poisson's ratio.[38] The expected wave speeds for the three plates studied are all subsonic (slower than the speed of sound in air) with the exception of the wave speeds in the 6.35 mm plate above 1880 Hz. As the bending wave speed increases, the radiation efficiency of the sound generated by these waves traveling in the plate generally increases (for the subsonic wave speeds).[38] This is the reason why thicker plates and higher frequencies are heard better and result in a shrill sound quality because of the higher bending wave speeds. Thus, the thinner plates are more desirable for the museum demonstration because the noise made by the demonstration can be annoying for users and others nearby. However, if the plate is too thin, then it is not structurally stable enough to support the weight of the equipment for the demonstration. From these experiments, it was concluded that the 1.27 mm thick plate was optimal.

### B. Frequency range and bandwidth

Next, the interaction between the plate and target LEGO minifigure was optimized. When the downward acceleration of the plate underneath the minifigure exceeds the acceleration due to gravity, the minifigure loses contact with the plate. Thus, if the downward acceleration exceeds 9.8 m/s$^2$ just prior to the TR focusing peak, then the minifigure is not maximally launched into the air, leading to the repeatability problem described in Sec. II. Thus, reducing the acceleration of the plate prior to the arrival of the focusing peak increases the amount of time that the minifigure is in contact with the plate and the likelihood that the minifigure will be hit by the main focal peak and be launched off of the plate. The acceleration amplitude, $a(t)$, in a time-harmonic motion is a function of the velocity amplitude, $v(t)$, and angular frequency, $\omega$,

$$a(t) = \omega v(t). \tag{6}$$

A parametric study was conducted on the amplitude, frequency range, and bandwidth to find the optimal values for both of these parameters. The optimal values of the amplitude, frequency range, and bandwidth are defined as the values that lead to the target minifigure being knocked over most repeatably while leaving the other nontarget minifigures on the plate standing. There are trade-offs, however, with the amplitude and frequency. Lower amplitudes and lower frequencies decrease the acceleration of the plate, but the amplitude still needs to be high enough to launch the target minifigure during the main focal event, and high frequencies are desirable because they increase the spatial confinement of the TR focusing, reducing the likelihood of the nearby minifigures being knocked over.

First, repeatability as a function of the frequency range of the chirp signal was studied, i.e., whether low, mid, or high frequencies are most important. These repeatability experiments were conducted with a set of fixed frequency bandwidths (each of 1000 Hz), but the range of the frequencies was changed (the starting and ending frequencies were changed by the same amounts). The chirp signal used to get the impulse response was set to a fixed bandwidth of 1000 Hz. A set of 40 trials were performed for each of the 12 different frequency ranges with the starting frequencies ranging from 100 to 1200 Hz in 100 Hz intervals [Fig. 4(a) gives the starting and ending frequencies for all of the ranges tested]. These experiments were performed on a 0.91 m × 1.22 m × 1.27 mm aluminum plate with four shakers and a SLDV. In an individual trial, the forward and backward steps of the TR were conducted and then a LEGO minifigure was placed at the focal location to see if it would be knocked over. Nine additional minifigures were placed at other locations on the plate at least 10 cm away from the shakers and the focal location. A successful trial was one in which the target minifigure was knocked over (fell down). The results of these fixed-bandwidth, varying-range experiments are shown as percentages of the success (repeatability) in Fig. 4(a) with 100% meaning that the target minifigure was knocked over 40 out of 40 times. Note that the results in Fig. 4(a) represent $12 \times 40 = 480$ individual trials of the demonstration. The results indicate that the 1000 Hz ranges at the lower frequencies were more effective in launching the target minifigure, and the success rate (or repeatability) dropped off quickly as the frequency increased.

To explore the effects of varying the bandwidth with a fixed starting frequency, 40-trial repeatability experiments were performed for 9 different bandwidths with each starting at 100 Hz but ending at frequencies ranging from 400 Hz to 10 kHz. Figure 4(a) shows that the lower frequency ranges are better, but Fig. 4(b) shows that the inclusion of

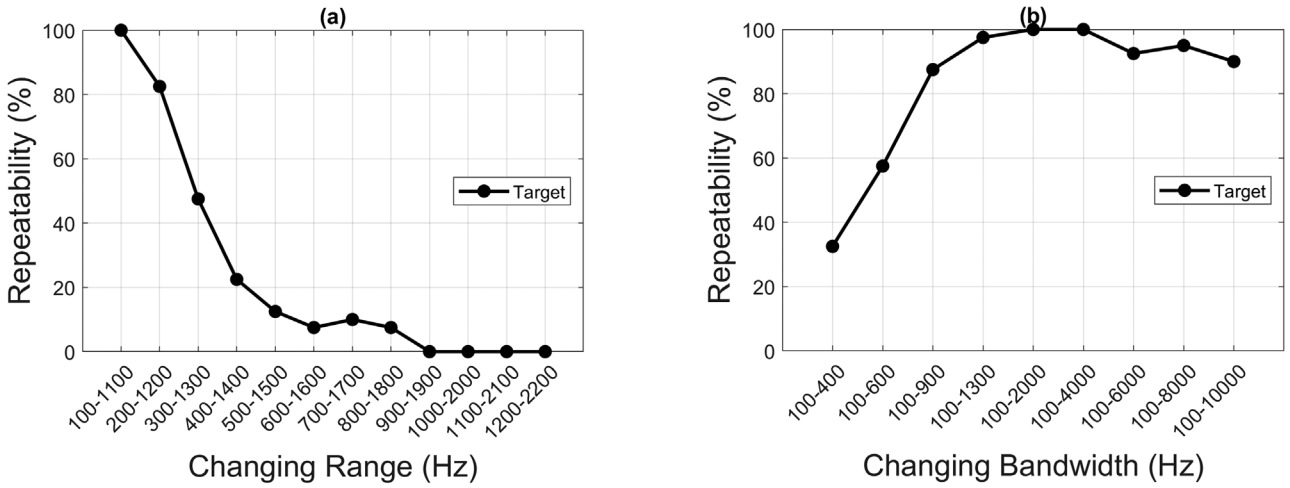


FIG. 4. The repeatability tests of the demonstration. Each data point represents the success rate (repeatability percentage) from 40 trials to knock over the target minifigure. The (a) repeatability when using various fixed frequency bandwidths of 1000 Hz while varying the range of the frequencies, and (b) repeatability when varying the bandwidth are depicted.

the higher frequency content (a wider bandwidth) increases the repeatability.

### C. TRIR amplitude

Next, a similar set of repeatability experiments were conducted for the different TRIR broadcast amplitudes to understand the effect of the amplitude on the repeatability of the demonstration. At this point, the 1.27 mm thick plate had been cut and bent into the shape of a bridge because the museum demonstration would use a bridge-shaped plate (one potential application of TR, which visitors could understand, is to detect and locate cracks in bridges and other structures). The TR experiments were performed starting with a low amplitude TRIR, which rarely knocked over the target minifigure and was not strong enough to ever knock any of the other minifigures over. For each of 12 different input amplitudes, 40 trials were performed. These repeatability results are shown in Fig. 5. The SLDV was again used along with a frequency bandwidth of 100–2000 Hz.

Although the specific input voltages greatly depend on the instrumentation used, the experimental results in Fig. 5 illustrate that a certain amplitude threshold is needed to repeatedly knock over the target minifigure. However, too much amplitude actually reduces the likelihood that the target will be knocked over and increases the likelihood of knocking over the other minifigures. The reduction of knocking over the target and the increase in knocking over nontarget minifigures can be explained by the higher amplitude sidelobes caused by a higher output amplitude from the shakers. The higher amplitude sidelobes can cause the target minifigure to be in the air when the main focal event happens, and the higher sidelobes will correspond to larger vibrations elsewhere in the plate, knocking over the nontarget minifigures. It is important to note that because the museum exhibit will only use two shakers, these repeatability versus amplitude experiments were done with two shakers, whereas the repeatability versus frequency experiments were done using four shakers. Using less shakers is the main reason why the highest repeatability achieved in these experiments was 92.5% (37/40) despite being performed with a bandwidth of 100–2000 Hz, which achieved 100% repeatability in the previous experiments [see Fig. 4(b)].

Based on the optimization experiments for the plate thickness, input amplitude, fixed bandwidth, and varying bandwidth, the optimal parameters for this specific setup with two shakers were determined to be 1.27 mm plate thickness, 1.5 V input amplitude to the shakers, and 100–2000 Hz frequency range for the chirp signal. With these optimal parameters, a repeatability of 92.5% was achieved. When using 4 shakers instead of 2 and an input voltage of 1 V, 100% repeatability was achieved for a set of 80 trials.

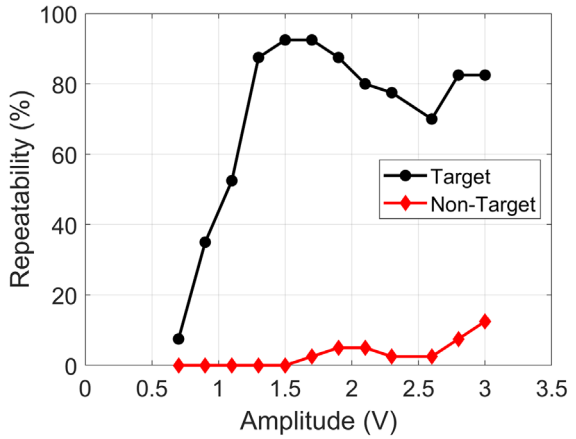


FIG. 5. (Color online) The repeatability of the demonstration when using different input amplitudes to the shaker sources. Here, the percentage of the times that the target minifigure was knocked over is tracked as well as the percentage of the times that the nontarget minifigures fell down. Each data point represents the success rate (repeatability percentage) for 40 trials conducted at each input amplitude. The SLDV was used here to create the velocity foci for these experiments.

https://doi.org/10.1121/10.0009364

## IV. USING DIFFERENT SENSORS BETWEEN STEPS OF THE TR PROCESS

The SLDV was used for all of the laboratory experiments previously discussed, but it is too expensive to use in a practical demonstration setting such as the planned museum exhibit. The SLDV is a velocity sensor, meaning that throughout the usable frequency bandwidth of the SLDV, the voltage output is proportional to the velocity of the plate. The SLDV shines monochromatic light at a vibrating surface, and some of this light must be reflected back to the SLDV's detector. The vibrating surface dynamically changes the frequency of the reflected light as the surface moves because of the Doppler effect. A comparison between the incident light and reflected light yields the velocity amplitude as a function of the time.

One relatively inexpensive sensor that was still able to measure the 100–2000 Hz frequency range adequately was an ECS, which is a noncontact displacement sensor. The ECS uses an active coil of wire to generate an alternating magnetic field in the vicinity of a conducting surface. The magnetic field causes small electric currents, called eddy currents, to be induced in the conductive surface, in this case, an aluminum plate. These eddy currents oppose the excitation current and cause a drop in the voltage across the sensor, which is measured and converted to an output voltage that is proportional to the displacement between the plate and sensor head. An additional advantage of the ECS over the SLDV is its portability, which is useful for performing this demonstration in various venues with ease. The purpose of this section is to contrast the use of the ECS (approximate cost $1.3k USD), a displacement sensor, to that of the SLDV (approximate cost $250k USD), a velocity sensor, in the TR experiments.

The ECS sensor used here is a Micro-Epsilon DT3001-U8-A-SA eddy current measuring system (Ortenburg, Germany) with a sensing range of 8 mm from the ECS surface. Because the ECS outputs a voltage proportional to the displacement relative to the sensing head, the signal response has a direct current (DC) offset [Fig. 6(a)], corresponding to the overall distance between the plate and ECS. The DC offset was removed by subtracting the mean of the dynamic signal recordings as in the chirp response pictured in Fig. 6(b). The ECS measurement range corresponds to an output voltage range from 0.5 to 9.5 V. To allow for the motion of the plate toward and away from equilibrium, it is optimal to place the plate well within the measuring range such that the alternating current (AC) voltages will not exceed the dynamic range of the digitizer card. This ECS also picks up quite a bit of low frequency noise, therefore, a second-order Butterworth filter, which had a bandpass response between 100 and 2000 Hz, was used to filter the signal response, as shown in Fig. 6(c). After removing the DC offset and filtering the chirp response signal, the cross correlation is performed to obtain the impulse response.

Because the ECS is a displacement sensor, the impulse response obtained between the shaker and ECS is a displacement signal. Thus, the use of this impulse response results in a TR focus that has a displacement peak [Fig. 7(a)]. If this displacement focus is recorded using a velocity sensor, such as a SLDV, the signal would instead show up as the "*N*-shaped" time derivative of the displacement focus signal [Fig. 7(b)]. If a SLDV is used to obtain the impulse response, which is subsequently used to create a TR focus, a SLDV recording will show a standard symmetric TR focus, which has a velocity peak [Fig. 7(d)]. A displacement recording of that velocity TR focus will appear as a backwards *N*-shaped time integral of that focus signal [Fig. 7(c)].

It is conceivable that the ESC could be used to create a backwards *N*-shaped displacement focus signal, similar to the one in Fig. 7(c), by modifying the displacement impulse response. This would allow a peak velocity to be created during the focusing. One way to create a backwards *N*-shaped focus and mimic the phase shift that an integral imposes would be to introduce a phase shift of −90° at all frequencies in the spectrum of the TRIR. The displacement during this TR focusing would look similar to that pictured in Fig. 7(c), but the velocity would look like that pictured in Fig. 7(d). A velocity sensor could be used with a modified impulse response to create a focusing like that pictured in Fig. 7(b) to create a displacement peak in the focusing like that pictured in Fig. 7(a). Applying a 90° phase shift to the velocity TRIR would create a velocity signal like that shown

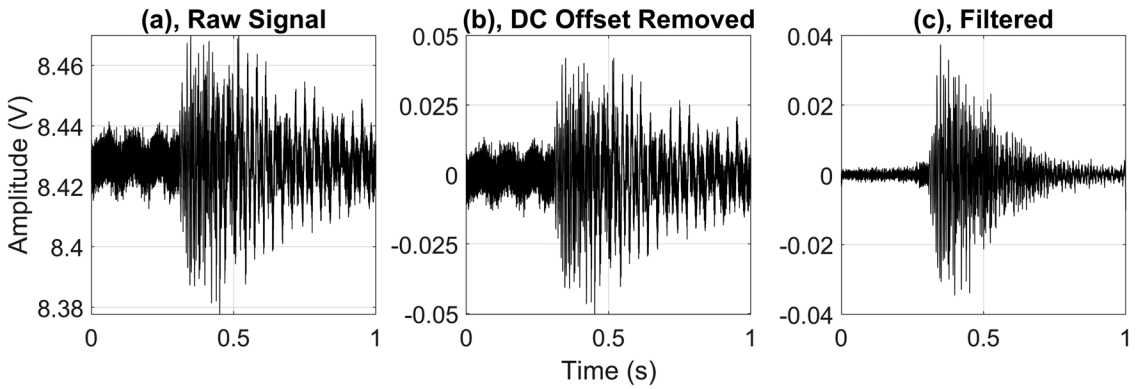


FIG. 6. The example signals recorded with the ECS. The (a) unfiltered chirp response with the DC offset, (b) unfiltered chirp response with the DC offset removed, and (c) filtered chirp response with the DC offset removed are shown.

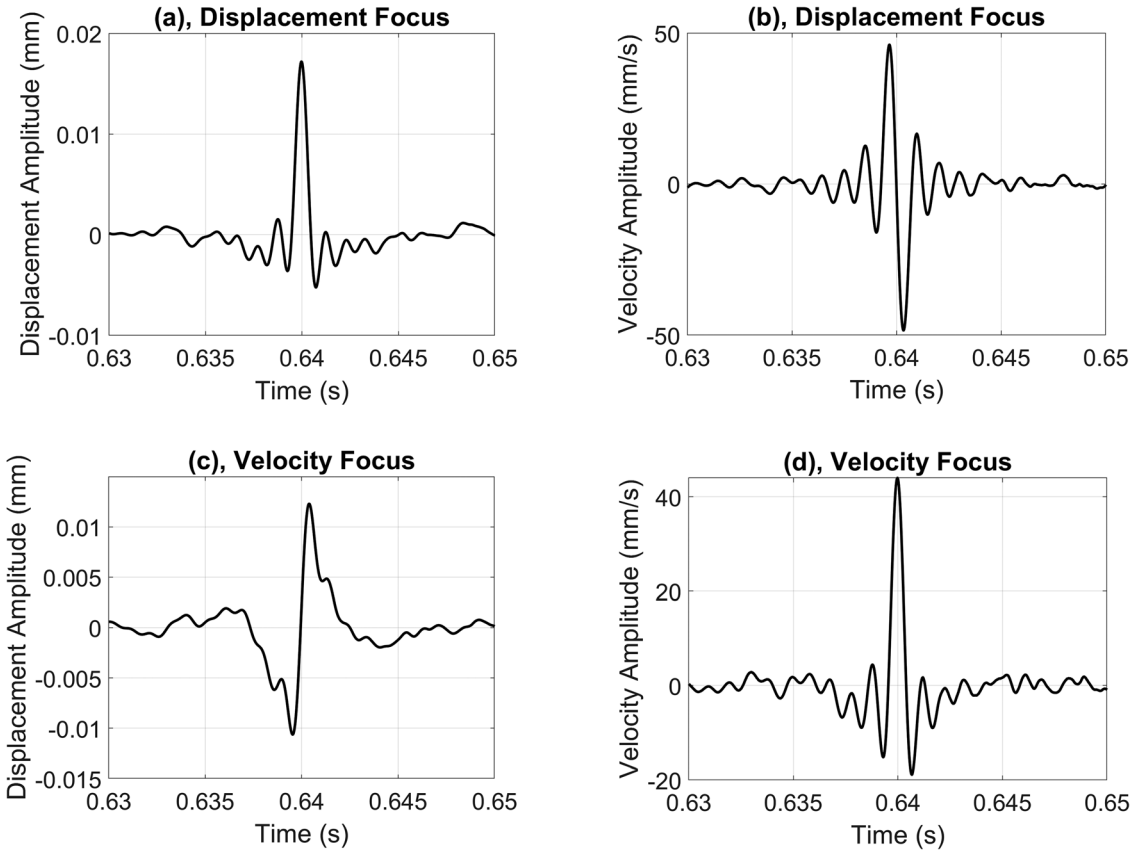


FIG. 7. The (a) displacement amplitude recording during the displacement TR focusing, (b) velocity amplitude recording during the displacement TR focusing, (c) displacement amplitude recording during the velocity TR focusing, and (d) velocity amplitude recording during the velocity TR focusing are shown.

in Fig. 7(b) during the TR focusing, whereas the displacement signal would look like that shown in Fig. 7(a). An accelerometer or another acceleration-based vibration sensor may also be used to create a displacement or velocity TR focus peak by applying a 180° or 90° phase shift to the TRIR, respectively. The authors verified that each of these experiments work as described by using the ECS and SLDV. A similar idea, called phase inversion or pulse inversion, introduced the idea of applying a 180° phase shift to the TRIR to create a symmetric, negative-value, TR focus peak.[39] Third-order phase symmetry analysis introduced the idea of implementing 120° and 240° phase shifts to the TRIR so that the 0°, 120°, and 240° phase shifted TRIR signals could be used to create three different focal signals, which may be combined in such a way to detect the presence of even or odd harmonics caused by the nonlinearities in a high amplitude TR focus.[40]

With the ability to create the different shaped focal signals comes the question of what focal shape will launch a LEGO minifigure the highest into the air to increase the chances of knocking over the minifigure? In Sec. III, it was found that the lower velocity and acceleration amplitudes were desirable to reduce the likelihood of the LEGO minifigure losing contact with the plate and being in the air when the focus peak arrives. The optimal, local motion of the plate would be a large upward velocity to give the minifigure a large upward momentum followed by a large downward acceleration (steep negative slope of velocity versus time) such that the minifigure would lose contact with the plate, and the plate would travel downward while the minifigure continued to rise further above the plate. The higher the minifigure travels, the more likely it will be to fall over on returning to the plate surface.

Because the displacement focus and velocity focus, measured in the velocity [Figs. 7(b) and 7(d), respectively], exhibit a large, positive-velocity peak followed by a large negative slope, it is expected that both types of foci could launch a LEGO minifigure. The experiments confirmed that a displacement focus and velocity focus were equally capable of launching the LEGO minifigure and knocking it over. In comparing Fig. 8 with Fig. 5, it can be seen that the ECS provided a similar overall repeatability trend as for the experiments performed with the SLDV in Sec. III with a set of 40-trial repeatability tests. These repeatability trials were also performed with only two shakers on the bridge-shaped plate as was performed with the SLDV repeatability versus amplitude trials. Using the ECS and two shakers on the bridge, the demonstration had a repeatability up to 92.5% (37/40) at an input voltage of 1.8 V to the shakers, which is the same maximum repeatability achieved with the SLDV and two shakers on the bridge. We expect that the findings for the plate thickness and general findings of the frequency optimization work hold when using the ECS instead of the SLDV. Some brief optimization checks were performed

https://doi.org/10.1121/10.0009364

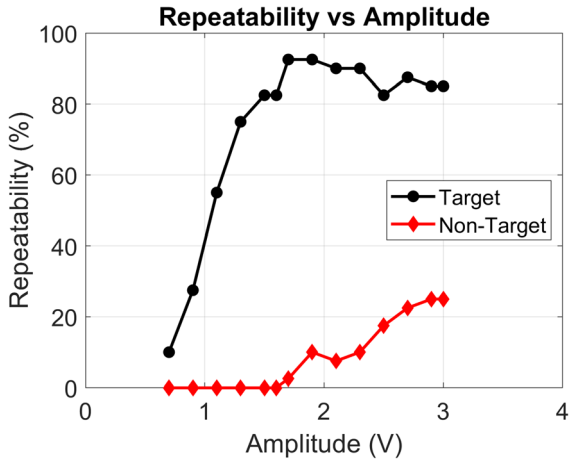


FIG. 8. (Color online) The repeatability of the demonstration when using different input amplitudes to the shaker sources. Here, the percentage of the times that the target minifigure was knocked over is tracked as well as the percentage of the times that the nontarget minifigures fell down. Each data point represents the success rate (repeatability percentage) for 40 trials conducted at each input amplitude. The ECS was used here to create the displacement foci for these experiments.

with the ECS to determine that the optimizations performed with the SLDV still held when using the ECS.

Whereas the low frequencies were found to contribute significantly to the successful launching of the target minifigure, they also have larger wavelengths and lead to a wider spatial focus. This is not desirable because a larger focal area will be more likely to knock over the nontarget minifigures. Because the ECS is more sensitive to the lower frequency motion than the SLDV, the spatial extent of the focusing was a concern. Also, as the ECS induces currents in the target material, the manufacturer states that the required sensing area is about 3–5 cm in diameter, which is much larger than the sensing area of the SLDV ($\sim$30 $\mu$m). This larger sensing area of the ECS also likely contributes to a wider focus. Heaton *et al.*[32] showed what the velocity profile of a velocity focus looks like. For comparison, in Fig. 9, the displacement profile of a displacement focus at the time of the maximal focusing using the ECS is shown. Note that

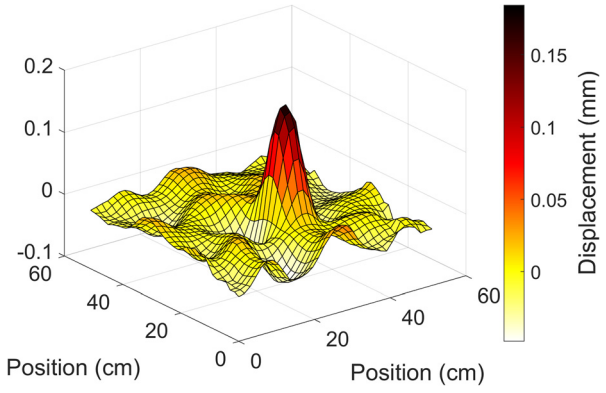


FIG. 9. (Color online) The surface plot of a displacement TR focus peak during the time of peak focusing. An ECS was used to obtain the impulse response and a SLDV was used to record the displacement at each scan position.

the scan area was 51 $\times$ 51 cm, and the flat, top surface of the bridge-shaped plate was 61 $\times$ 91 cm in area. The full width at half maximum of this displacement focus was determined to be 6.2 cm.

## V. MUSEUM EXHIBIT

This section will focus on describing how the demonstration was made more practical and cheaper for the museum exhibit "Waves" at *focus*Terra, the Earth and Science Discovery Center of ETH Zurich, Switzerland.[41] The "Waves" exhibition showcases the many facets of wave phenomena in daily life.[42] The exhibition allows visitors to playfully and experimentally explore the characteristics of the waves and how they are used in nature and technology. Figure 10(a) shows a bird's eye view of the exhibition. TR is a great example of focusing energy via waves and, thus, the demonstration described and optimized throughout this work was a perfect fit for the "Waves" exhibition. The visitors are shown videos of the wave propagation during the forward (Mm. 1) and backward steps, focused to two different locations (Mm. 2 and Mm. 3, respectively) as obtained by a SLDV and slowed down for visualization purposes.

Mm. 1. Video presented to the museum visitor, which describes the forward propagation step of the demonstration during the broadcast of the chirp signals. A video of the vibrations as acquired with a scanning laser vibrometer is shown. This is a file of type "mp4" (9.3 MB).

Mm. 2. Video presented to the museum visitor, which describes the backward propagation step of the demonstration during the broadcast of the reversed impulse responses. A video of the vibrations as acquired with a scanning laser vibrometer is shown for the focus position A. This is a file of type "mp4" (8.0 MB).

Mm. 3. Video presented to the museum visitor, which describes the backward propagation step of the demonstration during the broadcast of the reversed impulse responses. A video of the vibrations as acquired with a scanning laser vibrometer is shown for the focus position B. This is a file of type "mp4" (7.5 MB).

For the museum exhibit setup, a bridge-shaped aluminum plate with a thickness of 1.5 mm and top surface measuring 91 cm $\times$ 61 cm was used. The bridge shape illustrates a possible application in which the TR may be used. Two Mighty Dwarf 7W shakers were placed at an offset at opposite ends of the bridge. Less output channels meant lower cost, but this also decreased the repeatability of the demonstration somewhat. The ECS was mounted on three computer-controlled FUYU FSL40 linear motion stages (Chengdu City, China) in the shape of an "*H*" so that the ECS can be translated in two dimensions underneath the plate and acquire the necessary displacement recordings.

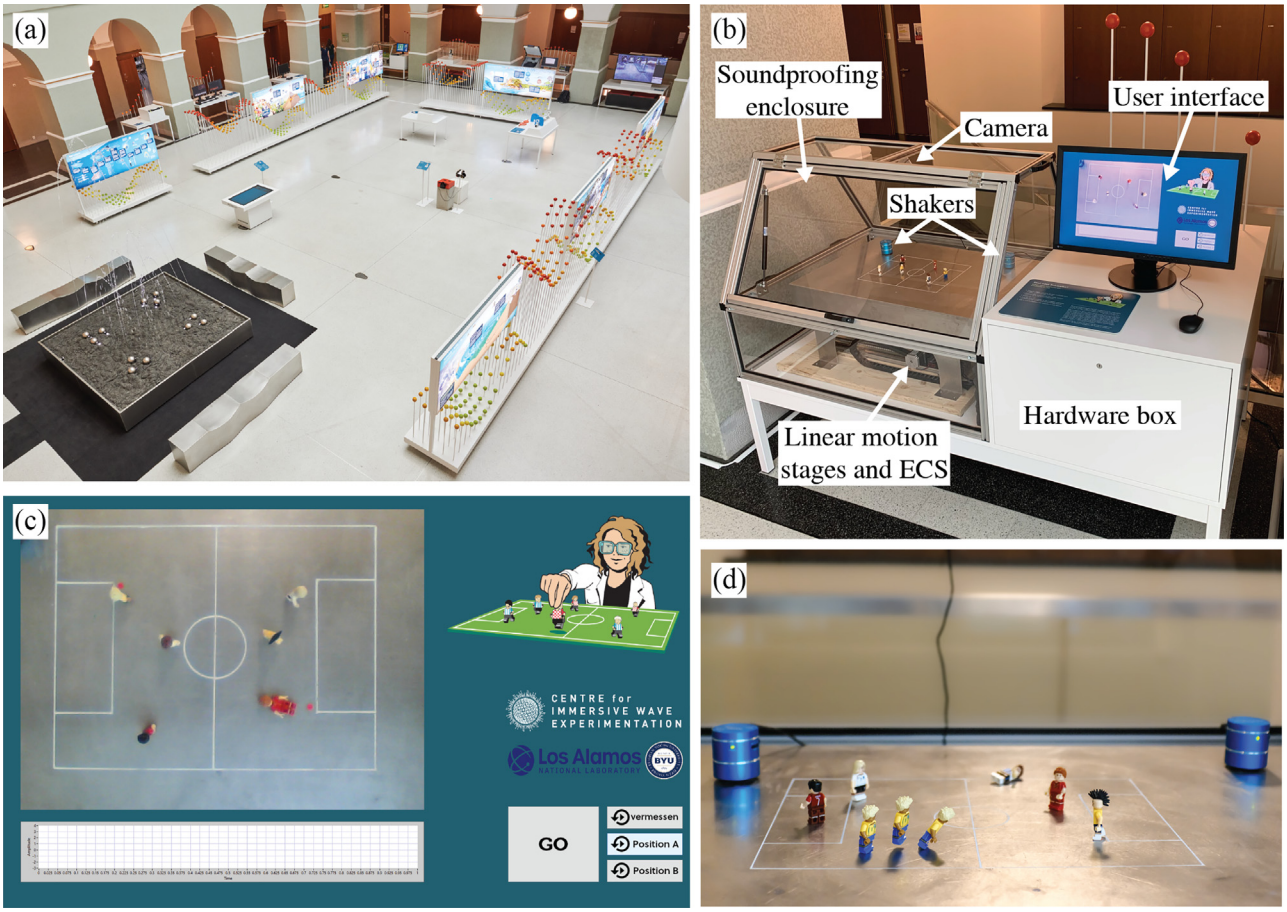


FIG. 10. (Color online) The (a) "Waves" exhibition at *focus*Terra (Courtesy of Matthias Auer of *focus*Terra), and (b) TR demonstration described in this work, found in the upper left corner of the exhibition [see (a)], are depicted. The aluminum table with the two shakers and LEGO minifigures is enclosed by a soundproofing enclosure. (c) The user interface requires the visitors of the museum to first select a LEGO minifigure on the soccer field and then press "GO." The ECS below the aluminum plate then records the impulse response at the location of the target minifigure while successively exciting the two shakers. After which, the TRIR is broadcast. (d) The overlay of the three consecutive photographs shows a targeted Lego minifigure jumping and falling due to the TRIR (courtesy of Matthias Auer of *focus*Terra).

The data acquisition and generation are managed with a National Instruments (Austin, TX) USB-6211 multifunction input/output device. This device had a lower amplitude resolution than the data acquisition cards used in the laboratory, and this reduced the temporal quality of the TR focusing somewhat, which reduced the repeatability some. The complete setup is shown in Fig. 10(b). A user interface, a screenshot of which is shown in Fig. 10(c), along with an overhead camera allows users to select a location on the plate where they want to create a TR focus. The translation stages underneath the plate then move the ECS to the selected location and a chirp is emitted in turn from each shaker while the ECS records the response between each shaker and the target location. The impulse responses are determined through filtering and cross correlation. Then, the ECS is moved away from the target location, and the two shakers simultaneously broadcast their respective TRIRs, creating a focus at the target location.

As shown in Figs. 10(b) and 10(c), the bridge is populated with LEGO minifigures, arranged to resemble two opposing soccer teams. The visitors to the museum exhibit then take turns trying to knock over the players of the other team using the TR focusing. The user interface, provides further information on how the TR aims to focus waves to a selected location and its application in science and industry. Moreover, the user can view three animations of the plate vibrations acquired with a SLDV system when sending the chirps and a TR focus at two fixed positions on the plate (the videos can be seen in Mm. 1–Mm. 3).

Of note is the Plexiglas enclosure covering the aluminum table visible in Fig. 10(b). The museum *focus*Terra is integrated into the Earth Science building. Thus, one requirement that the demonstration had to meet was to not disturb the students and employees working in the building. The findings introduced in this paper have allowed the demonstration to be much quieter than the previous version of the demonstration presented by Heaton *et al.*[32] The use of a thinner plate and reduced bandwidth both help to reduce the radiated noise. The deconvolution TR technique and the use of multiple shakers also allows smaller vibration amplitudes to be used while still yielding a sufficiently large focal amplitude to launch the minifigure. However, the noise broadcast by the shaker's interaction with the aluminum plate was still too loud. Consequently, a soundproofing

https://doi.org/10.1121/10.0009364

enclosure was designed and manufactured in cooperation with Kanya AG (Rüti, Switzerland) to ensure an acceptable noise emission. The enclosure can be opened at the front to allow users to place the minifigures on the soccer field (pitch). The camera is mounted at the top, directly above the soccer field. Moreover, 5 cm thick soni WAVE sound absorbing foam (Soniflex, Denmark), targeting sound absorption in the 400 Hz–5 kHz range) was attached to the lower back face (35 × 114 cm) and the face was adjacent to the hardware box (35 × 92 cm).

The sound pressure level (SPL) was then measured using the XL2 audio analyzer by NTI audio (Schaan, Liechtenstein) at a distance of 1 m and height of 1.5 m without and with the soundproofing enclosure present. Figure 11 shows a reduction in the SPL of 18.5 dB when emitting the chirps and a reduction in the SPL of 26.7 dB when the TRIR is introduced to the aluminum plate. As a result, using the soundproofing enclosure, the demonstration is quiet enough but still audible to the user when directly interacting with it. The latter point is important as it makes it easier for the user to establish the link between the waves and the focusing of energy.

The initial testing found that repeatable TR focusing results, i.e., the LEGO minifigure either jumping or falling, were only found when manually increasing the volume of the two Mighty Dwarf shakers to their maximum (this is required to do every time the shakers are powered on). However, this is not practical for an exhibition piece, which should require the least amount of maintenance possible. Thus, the output of the National Instruments USB-6211 (Austin, TX) is amplified by a Monacor SA-100 stereo amplifier (Bremen, Germany) prior to being sent to the Mighty Dwarf speakers. Also, in an effort to streamline the processing of the data, the experiment was tested without bandpass filtering the recordings. These factors led to a decrease in the repeatability compared to the repeatability of the laboratory demonstration at Brigham Young University (BYU), which was described previously. Further reduction in the repeatability was observed due to the user's accuracy when interacting with the demonstration and camera alignment precision. In other words, if the user does not exactly select where the target minifigure is or the positioning system for the ECS is not aligned with the camera view on the user interface, the target minifigure might not be standing at the exact TR focal spot.

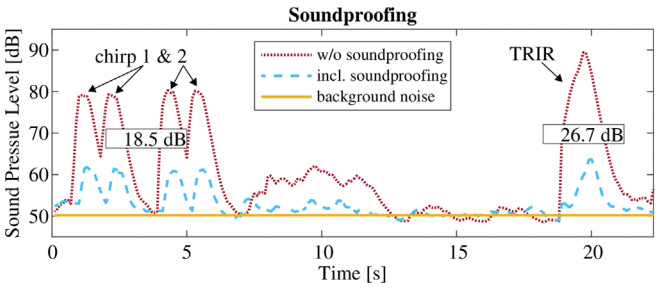


FIG. 11. (Color online) The difference in the sound pressure level as a function of time when covering the TR demonstration with a soundproofing enclosure. The (red) dotted line shows the measured SPL without the soundproofing enclosure. The (light blue) dashed line shows the drop in the SPL when covering the demonstration with the soundproofing enclosure. Each chirp is broadcast twice from each of the two shakers. After which, the TRIR signal is broadcast. A drop of 18.5 dB is measured for the chirps and 26.7 dB for the TRIR. Finally, the (yellow) line indicates the measured average background noise.

The settings for the exhibition are as follows. The chirp signals span a range from 100 Hz to 1.6 kHz and are played for a duration of 500 ms. Additionally, the signal measured by the ECS is averaged twice. It was found that the averaging leads to a better calculated TRIR as the ambient vibrations are a factor when the visitors interact with the exhibition. The amplitude of the TRIR emitted by the two shakers is 11.6 times as large as the amplitude of the initial chirps.

The repeatability was tested using these settings. Out of 40 trials, the target minifigure visibly jumped in the air 75% of the time but only fell over 30% of the time, and the non-target minifigures were knocked over 15% of the time. However, because the demonstration is presented in a game format, a decreased repeatability is desirable because it adds an element of unpredictability, which makes it more fun for the users. Figure 10(d) shows an example of a jumping and falling soccer player. When compared with Fig. 2(b), the minifigure does not jump as high. However, the desired effect of playfully and experimentally demonstrating the focusing of the energy in a medium via waves is clearly conveyed to the user.

## VI. CONCLUSION

This paper proves a better physical understanding and optimization of a demonstration of TR acoustics introduced by Heaton *et al.*[32] First, a comparison between the traditional TR, deconvolution TR, and clipping TR was presented. This led to the experimental discovery that large amplitude sidelobes were causing the target minifigure to bounce prematurely, sometimes causing it to be in the air during the main focal event and not be knocked over. This critical insight indicates that the best TR method to use for high repeatability in the demonstration is deconvolution because the deconvolution method leads to a better signal-to-noise ratio than is typical of traditional TR or clipping TR and, therefore, smaller sidelobes, while maintaining enough amplitude in the focus to launch the minifigure.

Several parameters of the setup and TR process were optimized, including the thickness of the plate, frequency range of the chirp, and amplitude of the TRIR. Three different plate thicknesses were studied, and it was found that the thinner plates yield higher peak amplitudes as well as a higher temporal quality. These are both desirable traits for a TR focal signal so long as the structure is strong enough to stand and support any required equipment. Additionally, less noise is radiated from the thinner plates because the waves are more likely to be traveling at subsonic speeds.

For the chirp frequency range optimizations, one set of repeatability experiments was performed while varying the upper bound of the chirp and holding the lower bound

constant, and another set of experiments were performed while holding the bandwidth constant and raising the lower and upper bounds of the chirp together. It was found that the lower frequencies are the most effective in knocking over the target minifigure, but the higher frequencies are also necessary to reduce the number of times the nontarget minifigures were knocked over by reducing the spatial extent of the focusing. In the end, the frequency range of 100–2000 Hz was determined to be optimal for the demonstration.

Another set of repeatability experiments was performed while varying the output amplitude of the TRIR. An important trade-off discovered was that there needs to be enough amplitude to knock over the target but too much amplitude would cause the sidelobes to be too large, and the minifigure could prematurely bounce into the air and miss the main focal event. Therefore, a balance must be found, but the specific amplitude will vary from setup to setup. The optimal parameters for our specific setup with two shakers were determined to be 1.27 mm plate thickness, 1.5 V input amplitude to the shakers, and 100–2000 Hz frequency range for the chirp signal. With these optimal parameters, a 92.5% repeatability for a set of 40 trials was achieved. Additionally, when using 4 shakers instead of 2 and an input voltage of 1 V, a 100% repeatability for a set of 80 trials was achieved.

The main differences in the state of the demonstration before and after the contributions of this paper are that the launch height of the minifigure is lower, which is quieter and much more repeatable, a cheaper sensor was implemented, and there are less nontarget minifigures falling over. These optimizations made the demonstration suitable for the implementation as an exhibit in a wave propagation museum at ETH Zurich in Switzerland. Due to the hardware limitations, the repeatability in the museum exhibit was 30%, which was lower than the repeatability found in the laboratory. Fortunately, the lower repeatability provides for a more fun game of chance, and the demonstration remains an effective way to visualize the focusing power of the TR acoustics.

Videos of the TR LEGO minifigure demonstration can be found in Refs. 43–45.

Reference 43 includes a description of the demonstration as narrated by B.E.A. Reference 44 shows the demonstration conducted in the BYU laboratory using an ECS, and illustrates the repeatability with these conditions. Reference 45 shows the focusing waves followed by the initial video of the first demonstration along with an optimal launch result as conducted in the BYU laboratory.

## ACKNOWLEDGMENTS

The funding was provided by BYU College of Physical and Mathematical Sciences. The authors also thank the *focus*Terra team for the opportunity to include the TR demonstration in the "Waves" exhibition. Furthermore, the authors thank Thomas Haag for his technical assistance in getting the demonstration ready for the exhibition.

[1]M. Fink, "Time reversed acoustics," Phys. Today **50**(3), 34–40 (1997).
[2]B. E. Anderson, M. Griffa, C. Larmat, T. J. Ulrich, and P. A. Johnson, "Time reversal," Acoust. Today **4**(1), 5–16 (2008).
[3]B. E. Anderson, M. C. Remillieux, P.-Y. Le Bas, and T. J. Ulrich, "Time reversal techniques," in *Nonlinear Acoustic Techniques for Nondestructive Evaluation*, 1st ed., edited by T. Kundu (Springer and Acoustical Society of America, New York, 2018), Chap. 14, pp. 547–581.
[4]A. Parvulescu and C. S. Clay, "Reproducibility of signal transmission in the ocean," Radio Elec. Eng. **29**, 223–228 (1965).
[5]C. S. Clay and B. E. Anderson, "Matched signals: The beginnings of time reversal," Proc. Mtgs. Acoust. **12**, 055001 (2011).
[6]M. Tanter, J.-L. Thomas, and M. Fink, "Time reversal and the inverse filter," J. Acoust. Soc. Am. **108**(1), 223–234 (2000).
[7]M. Tanter, J. F. Aubry, J. Gerber, J.-L. Thomas, and M. Fink, "Optimal focusing by spatiotemporal filter. I. Basic principles," J. Acoust. Soc. Am. **110**, 37–47 (2001).
[8]T. Gallot, S. Catheline, P. Roux, and M. Campillo, "A passive inverse filter for Green's function retrieval," J. Acoust. Soc. Am. **131**, EL21–EL27 (2012).
[9]B. E. Anderson, J. Douma, T. J. Ulrich, and R. Snieder, "Improving spatio-temporal focusing and source reconstruction through deconvolution," Wave Motion **52**, 151–159 (2015).
[10]M. Fink, "Time-reversal acoustics in biomedical engineering," Annu. Rev. Biomed. Eng. **5**(1), 465–497 (2003).
[11]M. Fink, "Time reversal and phase conjugation with acoustic waves: Industrial and medical applications," Lasers Electro-Opt. **3**, 2334–2335 (2005).
[12]M. L. Willardson, B. E. Anderson, S. M. Young, M. H. Denison, B. D. Patchett, and T. Akal, "Time reversal focusing of high amplitude sound in a reverberation chamber," J. Acoust. Soc. Am. **143**(2), 696–705 (2018).
[13]C. B. Wallace and B. E. Anderson, "High-amplitude time reversal focusing of airborne ultrasound to generate a focused nonlinear difference frequency," J. Acoust. Soc. Am. **150**(2), 1411–1423 (2021).
[14]P.-Y. Le Bas, M. C. Remillieux, L. Pieczonka, J. A. Ten Cate, B. E. Anderson, and T. J. Ulrich "Damage imaging in a laminated composite plate using an air-coupled time reversal mirror," Appl. Phys. Lett. **107**, 184102 (2015).
[15]M. Farin, C. Prada, and J. de Rosny, "Selective remote excitation of complex structures using time reversal in audible frequency range," J. Acoust. Soc. Am. **146**(4), 2510–2521 (2019).
[16]G. F. Edelmann, H. C. Song, S. Kim, W. S. Hodgkiss, W. A. Kuperman, and T. Akal, "Underwater acoustic communications using time reversal," IEEE J. Ocean. Eng. **30**(4), 852–864 (2005).
[17]G. Zhang, J. M. Hovem, D. Hefeng, and L. Liu, "Coherent underwater communication using passive time reversal over multipath channels," Appl. Acoust. **72**(7), 412–419 (2011).
[18]C. He, Q. Zhang, and J. Huang, "Passive time reversal communication with cyclic shift keying over underwater acoustic channels," Appl. Acoust. **96**(9), 132–138 (2015).
[19]B. E. Anderson, T. J. Ulrich, P.-Y. Le Bas, and J. A. Ten Cate, "Three dimensional time reversal communications in elastic media," J. Acoust. Soc. Am. **139**(2), EL25–EL30 (2016).
[20]C. Larmat, J.-P. Montagner, M. Fink, Y. Capdeville, A. Tourin, and E. Clevede, "Time-reversal imaging of seismic sources and applications to the great Sumatra earthquake," Geophys. Res. Lett. **33**(19), L19312, https://doi.org/10.1029/2006GL026336 (2006).
[21]C. Larmat, J. Tromp, Q. Liu, and J.-P. Montagner, "Time-reversal location of glacial earthquakes," J. Geophys. Res. **113**(B9), B09314, https://doi.org/10.1029/2008JB005607 (2008).
[22]C. Larmat, R. A. Guyer, and P. A. Johnson, "Tremor source location using time-reversal: Selecting the appropriate imaging field," Geophys. Res. Lett. **36**(22), L22304, https://doi.org/10.1029/2009GL040099 (2009).
[23]C. S. Larmat, R. A. Guyer, and P. A. Johnson, "Time-reversal methods in geophysics," Phys. Today **63**(8), 31–35 (2010).
[24]I. Rakotoarisoa, J. Fischer, V. Valeau, D. Marx, C. Prax, and L.-E. Brizzi, "Time-domain delay-and-sum beamforming for time-reversal detection of intermittent acoustic sources in flows," J. Acoust. Soc. Am. **136**(5), 2675–2686 (2014).
[25]A. Mimani, Z. Prime, C. J. Doolan, and P. R. Medwell, "A sponge-layer damping technique for aeroacoustic time-reversal," J. Sound Vib. **342**, 124–151 (2015).

[26]A. Mimani, Z. Prime, D. J. Moreau, and C. J. Doolan, "An experimental application of aeroacoustic time-reversal to the Aeolian tone," J. Acoust. Soc. Am. **139**(2), 740–763 (2016).
[27]T. J. Ulrich, P. A. Johnson, and A. Sutin, "Imaging nonlinear scatterers applying the time reversal mirror," J. Acoust. Soc. Am. **119**, 1514–1518 (2006).
[28]T. J. Ulrich, A. M. Sutin, R. A. Guyer, and P. A. Johnson, "Time reversal and nonlinear elastic wave spectroscopy TR NEWS techniques," Int. J. Nonlin. Mech. **43**, 209–216 (2008).
[29]B. E. Anderson, M. Griffa, T. J. Ulrich, P.-Y. Le Bas, R. A. Guyer, and P. A. Johnson, "Crack localization and characterization in solid media using time reversal techniques," Am. Rock Mech. Assoc., presented at the 44th U.S. Rock Mechanics Symposium and 5th U.S.-Canada Rock Mechanics Symposium, Salt Lake City, Utah, June 2010.
[30]M. Fink, "Time-reversed acoustics," Sci. Am. **281**(5), 91–97 (1999).
[31]P. C. de Mello, N. Pérez, J. C. Adamowski, and K. Nishimoto, "Wave focalization in a wave tank by using time reversal technique," Ocean Eng. **123**, 314–326 (2016).
[32]C. Heaton, B. E. Anderson, and S. M. Young, "Time reversal focusing of elastic waves in plates for educational demonstration purposes," J. Acoust. Soc. Am. **141**(2), 1084–1092 (2017).
[33]A. Derode, A. Tourin, and M. Fink, "Ultrasonic pulse compression with one-bit time reversal through multiple scattering," J. Appl. Phys. **85**(9), 6343–6352 (1999).
[34]G. Montaldo, P. Roux, A. Derode, C. Negreira, and M. Fink, "Generation of very high pressure pulses with 1-bit time reversal in a solid waveguide," J. Acoust. Soc. Am. **110**(6), 2849–2857 (2001).
[35]B. Van Damme, K. Van Den Abeele, Y. Li, and O. Bou Matar, "Time reversed acoustics techniques for elastic imaging in reverberant and nonreverberant media: An experimental study of the chaotic cavity transducer concept," J. Appl. Phys. **109**, 104910 (2011).
[36]B. E. Anderson, M. Clemens, and M. L. Willardson, "The effect of transducer directionality on time reversal focusing," J. Acoust. Soc. Am. **142**(1), EL95–El101 (2017).
[37]M. H. Denison and B. E. Anderson, "Time reversal acoustics applied to rooms of various reverberation times," J. Acoust. Soc. Am. **144**(6), 3055–3066 (2018).
[38]F. Fahy and P. Gardonio, *Sound and Structural Vibration, Radiation, Transmission and Response* (Academic, Cambridge, MA, 2007), Vol. 26, pp. 185–195.
[39]A. Sutin, B. Libbey, V. Kurtenoks, D. Fenneman, and A. Sarvazyan, "Nonlinear detection of land mines using wide bandwidth time-reversal techniques," Proc. SPIE **6217**, 398–409 (2006).
[40]F. Ciampa and M. Meo, "Nonlinear elastic imaging using reciprocal time reversal and third order symmetry analysis," J. Acoust. Soc. Am. **131**(6), 4316–4323 (2012).
[41]focusTerra, The Earth and Science Discovery Center of ETH Zurich, available at https://focusterra.ethz.ch/en/ (Last viewed September 20, 2021).
[42]foucsTerra, "Waves, dive in!," available at https://waves.ethz.ch/en/ (Last viewed September 20, 2021).
[43]The Brigham Young University video of the time reversal LEGO demonstration, available at https://youtu.be/tCuIRNyXi6s (Last viewed September 20, 2021).
[44]The time reversal LEGO demonstration conducted in the Brigham Young University laboratory showing repeatability with the eddy current sensor, available at https://youtu.be/xbbQZo-Us80 (Last viewed September 20, 2021).
[45]The wave propagation visualization, the first time reversal LEGO demonstration video, and an optimized launch demonstration, available at https://youtu.be/emgzUa3U5bg (Last viewed September 20, 2021).